applied sciences

MDPI

Article

Energy Evolution Analysis of Coal Fracture Damage Process Based on Digital Image Processing

Zhonghu Wu [1,2,3,*], Liping Li [1,2], Yili Lou [4] and Wentao Wang [3]

[1] School of Qilu Transportation, Shandong University, Jinan 250002, China; yuliyangfan@163.com
[2] Geotechnical and Structural Engineering Research Center, Shandong University, Jinan 250061, China
[3] College of Civil Engineering, Guizhou University, Guiyang 550025, China; wangwentaogzu@163.com
[4] School of Civil Engineering, Central South University, Changsha 410004, China; louyiligzu@163.com
* Correspondence: wuzhonghugzu@163.com

Abstract: Coal rocks often contain calcite, which has a significant effect on the mechanical properties of coal and the energy evolution during rupture damage. In this study, the meso-scale of rock is considered, and the spatial distribution of the internal structure of coal is characterized by digital image technology. Uniaxial compression tests were conducted using RFPA on coal rocks containing calcite veins with diverse dip angles. The research results show that the different azimuth angles of the calcite veins change the internal stress distribution of the coal, resulting in higher coal compressive strength at low dip angles (0°, 15° and 30°). Under high dip angles (45°, 60°, 75° and 90°), coal has lower compressive strength. The fracture mode of coal is significantly affected by calcite. At low dip angle, the fracture mode of coal and rock is complex, which are inclined Z-type (0°), V-type (15°) and inverted V-type (30°), respectively. At high dip angle, the fracture mode of coal and rock is single, which is type I failure mode. The destruction process of coal rocks is influenced by calcite veins. Under low dip angle, the internal stress distribution of coal is relatively uniform, the weak cementation between matrix and calcite vein in coal is not easy to be damaged, the stress required for coal failure is large and the input energy, accumulated elastic energy and impact energy index are large. Under high dip angle, the internal stress distribution of coal is uneven, the weak cementitious material between matrix and calcite vein in coal is easy to be damaged and the input energy, accumulated elastic energy and impact energy index are small.

Keywords: coal rock; RFPA; digital image; calcite vein; energy evolution

Citation: Wu, Z.; Li, L.; Lou, Y.; Wang, W. Energy Evolution Analysis of Coal Fracture Damage Process Based on Digital Image Processing. *Appl. Sci.* **2022**, *12*, 3944. https://doi.org/10.3390/app12083944

Academic Editors: Bin Gong, Tao Zhao and Hongyuan Liu

Received: 15 March 2022
Accepted: 9 April 2022
Published: 13 April 2022

1. Introduction

Coalbed methane (CBM) is often stored in coal rocks in an adsorbed state, and because of its extremely high calorific value and the fact that it produces almost no exhaust gas after combustion, it is a clean, unconventional energy source and a strategic national reserve resource [1–8]. Coal rocks are the main reservoir of CBM, and the mechanical properties of coal rocks and the energy analysis during fracture damage have been the key scientific problems in oil and gas development, as well as an important research direction in CBM exploration and development.

Coal rock is a mineral resource formed through a series of complex tectonic and geological processes, and is a key research target for national resource development. For the mechanical properties of coal rocks, scholars have done a lot of research work. It is found that the internal structural defects of coal are obvious, complex and changeable, and the dispersion is large, resulting in the low compressive strength of coal [9–15]. During the formation of coal under complex geological conditions, there are a large number of different meso-structures, such as mineral particles, holes and micro fractures. These meso-structures have a substantial effect on the mechanical properties and fracture damage processes of coal [16–19]. Liu et al. 2018 measured partial axial strains in coal rocks and

extrapolated partial axial strains from the overall axial strains in general agreement with the test results [20]. Zhao et al. (2015) treated coal rock as equivalent homogenized and constructed stress state expressions and proposed a general compression shear damage criterion considering the bond strength between coal and soft rock [21].

The fracture damage process of coal, like other rocks, is an unstable phenomenon of energy storage and release. The use of energy to analyze the damage process of rocks is gaining more attention in the theoretical and engineering communities [22–25]. Many scholars have conducted studies on the relationship between the energy released during the destruction of rocks and the damage, and fruitful results have been obtained [26,27]. In terms of experimental analysis, Giuseppe Ferro found no direct correlation between the effect of size on energy dissipation density and compressive strength [28]. While great progress has been made in rock energy evolution, many scholars are also committed to the study of coal energy release in mining [29–32].

As a complex natural heterogeneous material, coal is often filled with calcite veins under the action of geological structure. Complex calcite veins have crucial impacts on the mechanical properties, crack extension and energy evolution process of coal rocks. In the process of coal mining, understanding the mechanical properties, failure mode, energy input, accumulation, dissipation and release of coal is an important prerequisite for coal mine safety production. Many mine dynamic disasters are caused by the sudden release of a large amount of energy, such as common rock burst and mine earthquake [33,34]. Many coalbed methane mining processes are also achieved by inducing energy dissipation when coal seams are damaged. For example, coal seam cutting, pressure relief and permeability enhancement pumping is through the conversion of coal seam energy into more fracture surface energy [35,36]. Therefore, the research on the mechanical properties and fracture damage of calcite vein coal and rock has important theoretical guiding significance for the exploitation of coalbed methane.

In this paper, the calcite-bearing vein coal rocks of Laofang and Enhong in Yunnan are studied, and the internal structure of coal rocks is characterized by digital image technology for spatial distribution. Numerical models of coal rocks with seven sets of calcite veins of different azimuths were established using RFPA2D-DIP, and uniaxial compression tests were conducted under diverse loading conditions. The effect of calcite veins on the mechanical traits of coal rocks is studied in the paper, and how different calcite vein inclination angles affect the destruction process of coal rocks and the energy evolution traits are analyzed.

2. Numerical Model of Coal Based on Digital Image

2.1. Image Processing of Coal Rock Specimens

Digital image processing technology uses edge detection or threshold segmentation to divide different feature regions of the image. For different image features, the color space suitable for the feature can be selected for image segmentation [37]. In terms of rock materials, the HIS color space is often used for image segmentation. The HIS color space reflects a color model of human perceived color, and perceives color with hue, intensity and saturation [38].

In the process of building numerical models of coal rocks, digital image processing techniques are used to distinguish matrix from calcite in coal rocks. Most of the images of coal rocks are grayscale images, so the HIS color space is chosen to threshold the images of coal rocks for segmentation. Based on the color of the coal matrix and calcite veins (differentiated by I-value), a suitable threshold is chosen to split the coal matrix from the calcite.

Figure 1a shows the coal rock surface image filled with calcite. The coal rock image is taken from Laochang and Enhong blocks in eastern Yunnan. The size of the image is 230 × 230 pixels, and the actual size of the image is 50 mm × 50 mm. The coal matrix in the picture is black, and the calcite is white. Figure 1b shows the I-value variation curve on the AA′ scan line. Comparing Figure 1a,b, it is found that I values below 90 correspond

to coal rock matrix, and I values fluctuating above 90 correspond to calcite. Therefore, I = 90 is chosen as the threshold value to segment the image. Figure 1c shows the results after segmentation. In Figure 1c, yellow represents calcite, and blue represents coal rock matrix. Comparing Figure 1a,c, the spatial distribution of coal rock matrix and calcite vein can be accurately characterized after digital image processing.

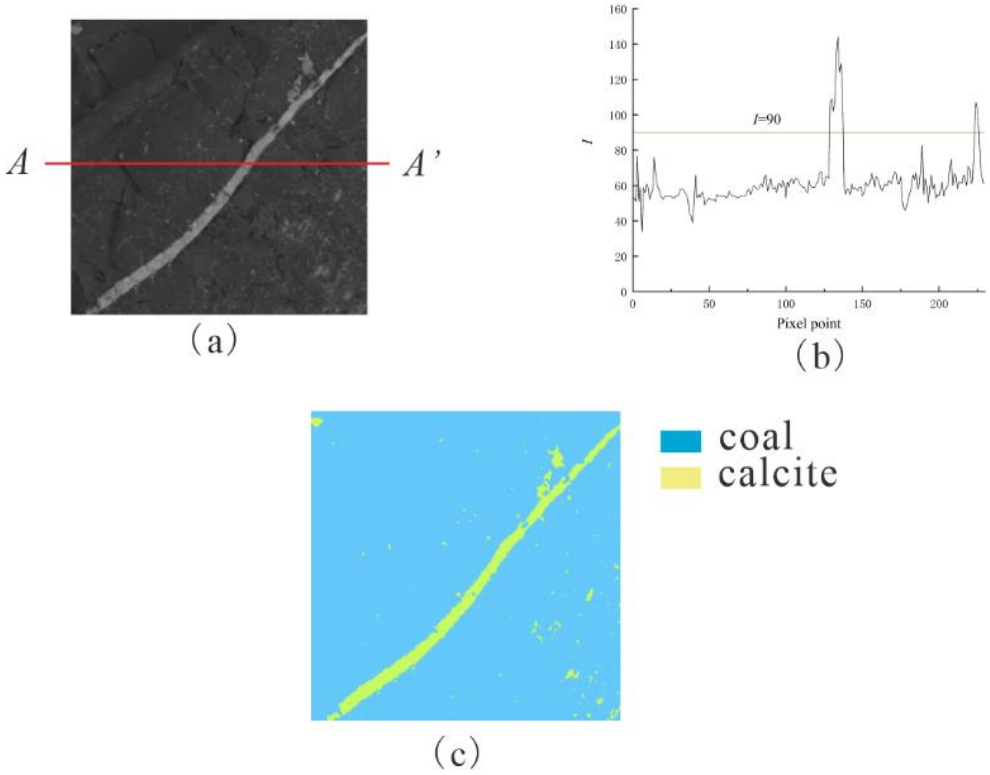

Figure 1. Calcite vein filled coal. (**a**) Surface image of coal; (**b**) change curve of *I* value on scan line *AA'*; (**c**) image after threshold segmentation.

2.2. Establishment of Numerical Model

The RFPA2D-DIP software is based on the RFPA2D, which, combined with digital image processing technology, through the characterization of material spatial distribution, establishes material numerical model and carries out numerical simulation test [39]. In RFPA2D-DIP, it is assumed that the meso unit mechanical parameters of coal matrix and calcite obey Weibull distribution [40]:

$$\psi = \frac{m}{n_0}\left(\frac{n}{n_0}\right)^{m-1} \exp\left[-\left(\frac{n}{n_0}\right)^{m}\right] \quad (1)$$

In Formula (1), n represents the mechanical parameters of the meso element; n_0 represents the average value of material meso units; m indicates the homogeneity of the rock particles, and the more homogeneous the particles are, the larger m is.

The calcite-bearing vein coal rocks were digitally imaged and numerically modeled as in Figure 2. The actual size of the model is 50 mm × 50 mm, and the unit divided into 230 × 230 = 52,900 meso units. Displacement loading is adopted for uniaxial compression numerical test, and the increment of each step is 0.002 mm/step. Table 1 lists the basic parameters of the coal rock matrix and calcite [41,42].

In studying the effect of calcite on the mechanical properties and damage process of coal rocks, seven sets of numerical models with different dip angles of calcite filled coal rocks were established. The numerical models are shown in Figure 3.

Table 1. Parameters of coal numerical model [41,42].

Material	Elastic Modulus E/MPa	Homogeneity *m*	Compressive Strength σc/MPa	Poisson Ratio ν	Internal Friction Angle (°)	Compressiontension Ratio
Coal	7000	5	60	0.40	35	10
Calcite	80,500	3	101	0.30	30	11

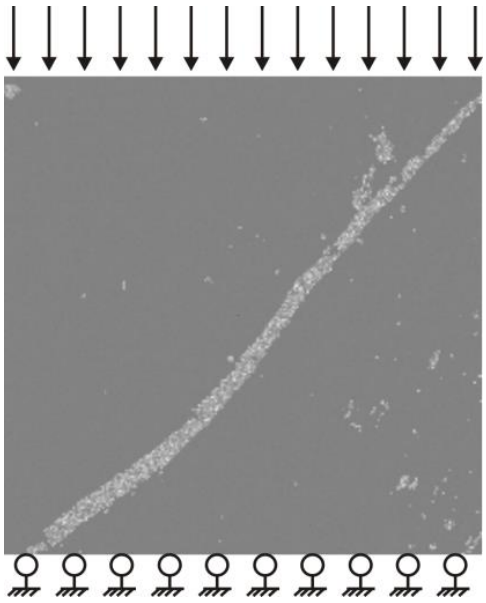

Figure 2. Loading diagram of coal and rock.

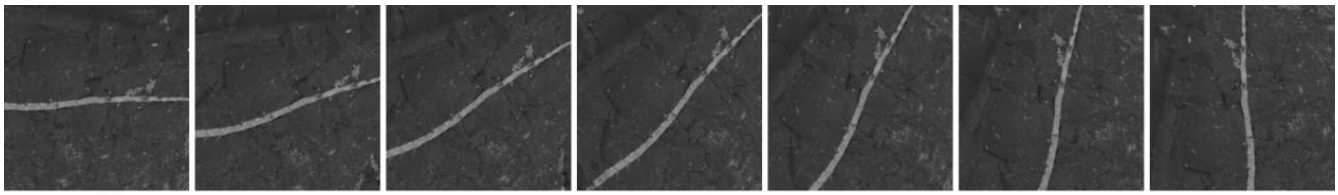

Figure 3. Digital images of coal and rock at different azimuth angles.

3. Analysis of Results

3.1. Mechanical Property Anisotropy Analysis

The test results are summarized in Table 2, where the compressive strength and elastic modulus of the coal rocks vary evidently with the disparate dip angles of the calcite veins. In order to be able to more visually reflect the effect of calcite veins on the overall mechanical properties producing anisotropy, the data in Table 2 are plotted in Figure 4.

Table 2. Modulus of elasticity and uniaxial compressive strength of coal rock.

Azimuth/(°)	Elastic Modulus/GPa	Uniaxial Compressive Strength/MPa
0	5.40	40.39
15	5.58	38.61
30	5.55	40.18
45	6.19	28.20
60	5.98	23.45
75	5.96	30.77
90	5.71	33.80

From Figure 4, it could be seen that both the compressive strength and elastic modulus of the coal show apparent anisotropy with the change of calcite vein dip angle α. When the calcite vein has low dip angle (0°, 15° and 30°), the compressive strength of coal is high, about 40 MPa. When calcite veins have high dip angles (45°, 60°, 75° and 90°), the compressive strength of coal is relatively low. When α = 0°, the maximum compressive strength of coal is 40.39 MPa; when α = 60°, it reaches the lowest value of 23.45 MPa, which is 41.94% lower than that of the 0° sample. This result is consistent with the strength effect of a single structural plane [43]. The trend of modulus of elasticity is opposite to the trend of compressive strength. When the calcite veins are of low dip angle, the modulus of elasticity of coal rocks is small. The modulus of elasticity is minimum at α = 0° with a value of 5.4 GPa. The modulus of elasticity of the kerogen is larger when the calcite veins are of high dip angle. When α = 45°, the modulus of elasticity is the highest, which is 6.19 GPa, which is 14.63% higher than that of the 0° sample. The reason for this phenomenon is that the presence of calcite veins affects the stress distribution in the coal rock. At low dip angle, the weak cementation between coal matrix and calcite vein is not easy to be damaged, resulting in high compressive strength. At high dip angle, the weak cementation between coal matrix and calcite vein is easy to be damaged, resulting in low compressive strength. Therefore, calcite vein has apparent results on the mechanical properties of coal.

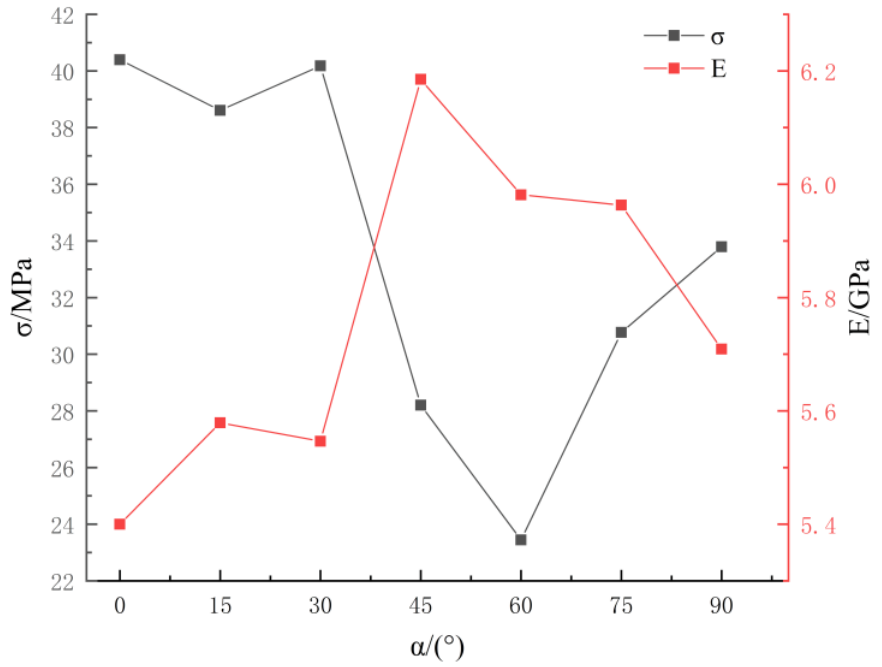

Figure 4. Compressive strength and elastic modulus of coal and rock at different azimuth angles.

Figure 5 shows the stress-strain curves of coal rocks containing calcite veins with diverse azimuth angles. From Figure 5, it can be seen that the deformation and damage process of coal rock has gone through three stages: linear elasticity, plasticity and failure. When calcite veins have a low dip angle, the strain from coal seam damage is large, while the strain from a high dip angle is small.

3.2. Failure and Deformation Characteristics of Coal Rocks

Figure 6 shows the stress distribution in the coal rock at a stress level of about 10%. The color brightness in the graph is positively correlated with the stress. From Figure 6, it can be seen that calcite veins with different dip angles reconfigure the internal stresses in the coal rock, which is also responsible for the change of mechanical properties in Section 3.1 of the coal rock.

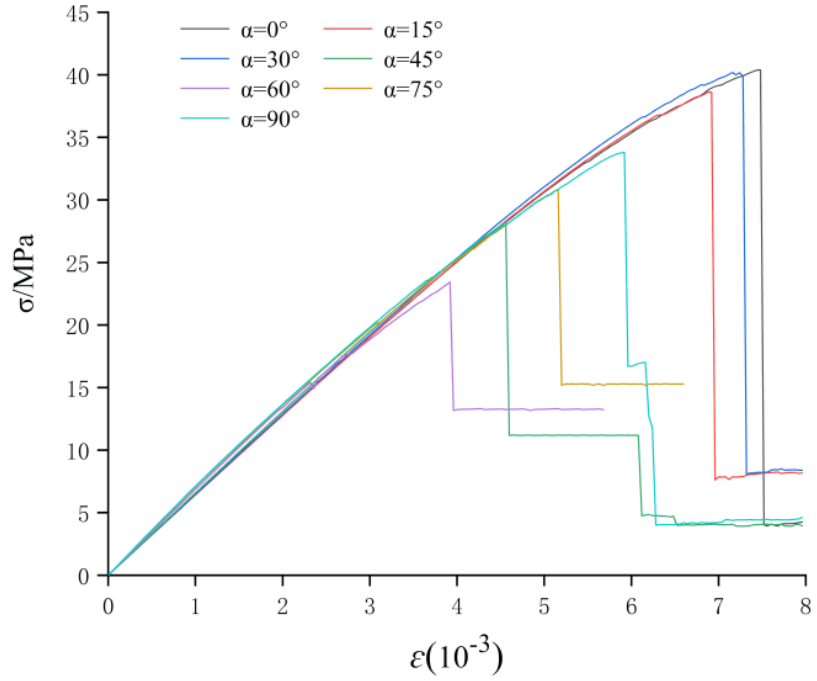

Figure 5. Stress−strain relation curves of coal and rock under diverse azimuth angles.

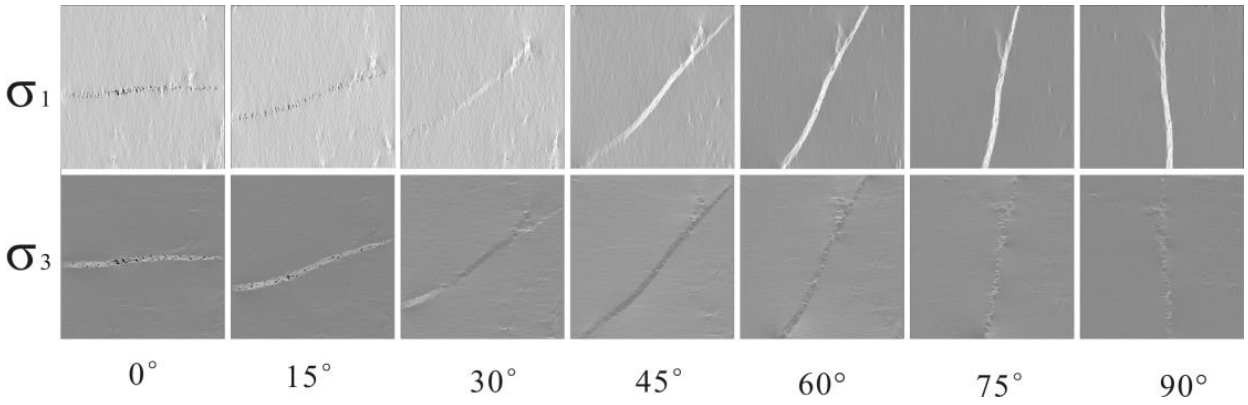

Figure 6. Stress distribution of coal with stress level of 10%.

Figure 7 shows the fracture process and acoustic emission diagram of coal in different directions. From Figure 7, we can find that calcite veins have a major effect on the destruction process of coal rocks, and tensile and shear damage mainly occur in the destruction process of coal rocks containing calcite veins. The crack distribution and final damage pattern of the kerogen are strongly influenced by the dip angle α of calcite veins and show strong variability.

1. When α = 0° and 15°, the cracks appeared first in the calcite veins, and the samples at 0° were uniformly distributed, and the results of the study were consistent with those of Taixu Bai and C.A. Tang [44,45]. When α > 15°, the initial crack initiated only locally in the calcite vein. When the azimuth angle is high (75° and 90°), the initial crack does not initiate vertically, but forms a certain included angle with the loading direction. It is worth noting that the equal-spacing cracks only appear when the inclination angle is low, but there are no equal-spacing cracks at the higher inclination angle. This may be due to the change in the inclination of the calcite veins and the change in the internal stress distribution of the coal, which in turn led to the above phenomenon.

2. When the calcite veins are at low inclination angles (0°, 15° and 30°), crack extensions appear in the calcite veins, forming a larger angle with the calcite veins, and finally forming complex fracture modes, which are respectively oblique Z-shaped (0°), V-shaped (15°) and inverted V-shaped (30°) failure modes, and mainly shear failure. When the calcite veins have high dip angles (45°, 60°, 75° and 90°), the fracture mode of the coal is single, which is a type I failure mode, and the angle with the calcite veins is small, mainly tensile failure. When α = 75° and 90°, the coal is almost completely destroyed along the calcite vein.

In the acoustic emission distribution in Figure 7, red indicates tensile failure, yellow indicates shear failure and black indicates failure. Generally speaking, the coal fracture process involves shear failure and tensile failure. When the dip angle of calcite veins is low (0°, 15° and 30°), there is more shear damage inside the specimen and some amount of tensile damage. When calcite veins have high dip angles (45°, 60°, 75° and 90°), the form of kerogen damage changes to tensile damage and shear damage occurs in small amounts, which is consistent with the results of the above analysis.

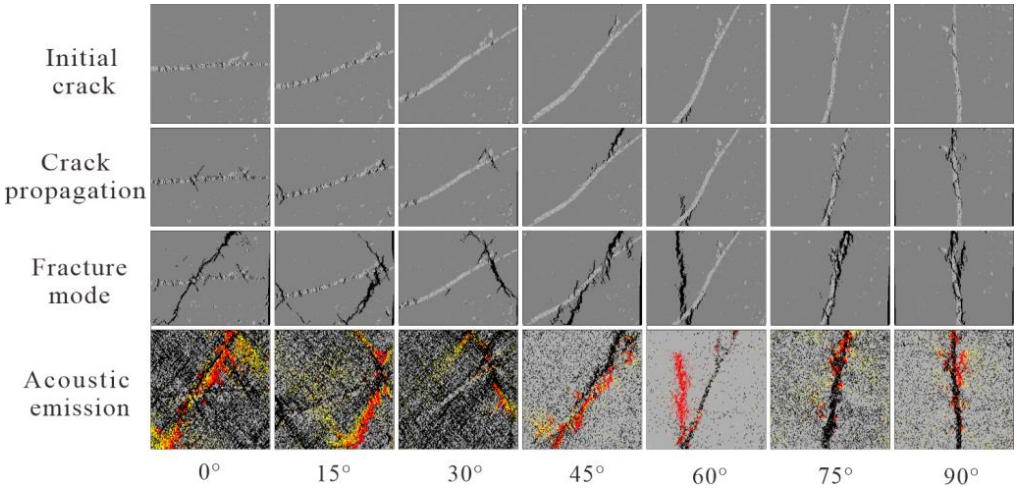

Figure 7. Fracture process and acoustic emission diagram of coal at different azimuth angles.

3.3. Analysis of Energy Evolution during Coal Fracture Damage

3.3.1. Coal Energy Evolution Characteristic Index

The energy value before and after rock fracture is closely related to its fracture mode. In fact, a series of energy indices (impact propensity indices) have been proposed and widely used in rock impact ground pressure and rock-burst studies to characterize the energy evolution of loaded rocks and to explain the magnitude and severity of rock fractures.

The more elastic energy the rock accumulates, the stronger its propensity to impact, the less energy it dissipates, and the more energy it releases when it breaks. The less elastic energy a rock accumulates, the less it exhibits a tendency to impact, the more energy it dissipates, and the less energy it releases when it breaks [46].

These characteristic indexes mainly include elastic energy index and impact energy index. In recent years, some scholars have proposed new indicators to correct the shortcomings of the above indicators, mainly including effective impact energy index, residual energy index, etc. these indicators are important manifestations of rock energy evolution characteristics.

Elastic energy index W_{ET} is defined as the ratio of elastic performance to energy consumption at 80–90% strength before the peak, as shown in Figure 8, $W_{ET} = S_{EAC}/S_{EOA}$. Its value shows a positive correlation with the impact propensity of the rock. The criteria determined by the Polish General Institute of mining research are: $W_{ET} \geq 5.0$ is strong impact tendency, $2.0 \leq W_{ET} < 5.0$ is medium impact tendency, and $W_{ET} < 2.0$ has no impact tendency.

The impact energy index K_E is defined as the ratio of the area under the stress-strain curve before and after the peak, as shown in Figure 8, $K_E = S_{OEFD}/S_{FDHG}$. The larger the value, the stronger the impact tendency. It is generally considered that $K_E > 2.0$ is a strong impact tendency, $1.0 \leq K_E < 2.0$ is a medium impact tendency and $K_E < 1.0$ has no impact tendency.

The effective impact energy index K_{eff} is the ratio of the elastic energy stored before the peak strength of the rock to the energy required for post-peak damage, with the expression $K_{eff} = S_{FBD}/S_{FDHG}$. S_{FBD} is the area under the peak unloading line FB in Figure 8, and S_{FDHG} is the area under the post-peak curve.

The expression for calculating the residual energy index W_R is $W_R = (S_{FBD} - S_{FDHG})/S_{FDHG}$.

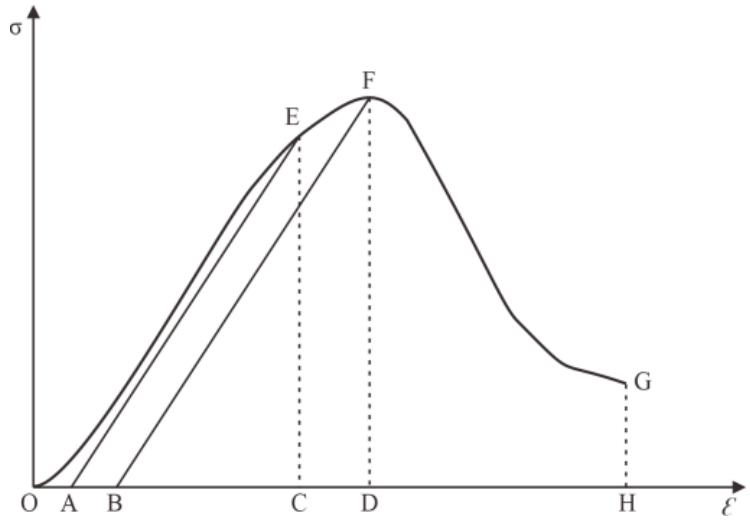

Figure 8. Rock energy characteristic index.

The characteristic energy parameters of each sample are calculated through the stress-strain curves of coal with 7 different calcite vein dip angles (see Figure 5), as shown in Table 3, and drawn into Figure 9. It was analyzed that:

1. With the rise of calcite vein dip angle, the input energy density before the peak value $E1$, the input energy density at 80% strength $E3$ and the accumulated elastic property density at 80% strength $E4$ show a change trend of first declining and then rising. In contrast, the pre-peak cumulative elastic energy density E2 exhibits a repeatedly increasing and then decreasing trend.
2. On the whole, when the angle of calcite vein is low, that is, the samples with low dip angle (0°, 15° and 30°), the input energy and accumulated elastic energy are large. The input energy and accumulated elastic energy of samples with high inclination angles (45°, 60°, 75° and 90°) are lower.

The reason for the above situation is that the coal is not easy to be damaged at low inclination angle, the number of loading steps is more, and more energy is required for damage.

The energy characteristic index of each sample is calculated by calculating the stress-strain curves of coal rock with 7 various calcite vein dip angles (see Figure 5), as shown in Table 4 and drawn into Figure 10. From Figure 10, we can find:

1. As the dip angle of calcite veins increases, the impact energy index, effective impact energy index and residual energy index of coal first decrease sharply, with a minimum value at $\alpha = 60°$, followed by a small increase. When $\alpha = 60°$, the effect energy index of coal rock is the smallest, which is 2.10. When $\alpha = 0°$, the impact energy index of coal is the largest, which is 36.27, 17.29 times that of 60° sample. When $\alpha = 0°$, the elastic energy index of coal is the smallest, which is 5.95. When $\alpha = 60°$, the effect energy index of coal is maximum, which is 27.14, which is 4.56 times that of 0° sample.

2. According to the results of 7 groups of tests, the elastic energy index of 7 groups of samples is greater than 5, the effect energy index is greater than 2 and the effect tendency of coal is strong.

Table 3. Characteristic energy parameters of coal at different azimuth angles.

α(°)	E_1/KJ*m^{-3}	E_2/KJ*m^{-3}	E_3/KJ*m^{-3}	E_4/KJ*m^{-3}
0	67.26	29.31	44.69	38.26
15	58.47	36.28	38.71	35.54
30	64.29	34.00	42.40	38.19
45	26.74	19.95	17.62	17.39
60	19.76	17.09	13.19	12.72
75	34.25	30.41	22.85	21.77
90	44.33	25.67	29.65	25.96

* E_1 is the input energy density before the peak; E_2 is the performance density of accumulation projectile before peak; E_3 is the input energy density at 80% strength; E_4 is the accumulated elastic performance density at 80% strength.

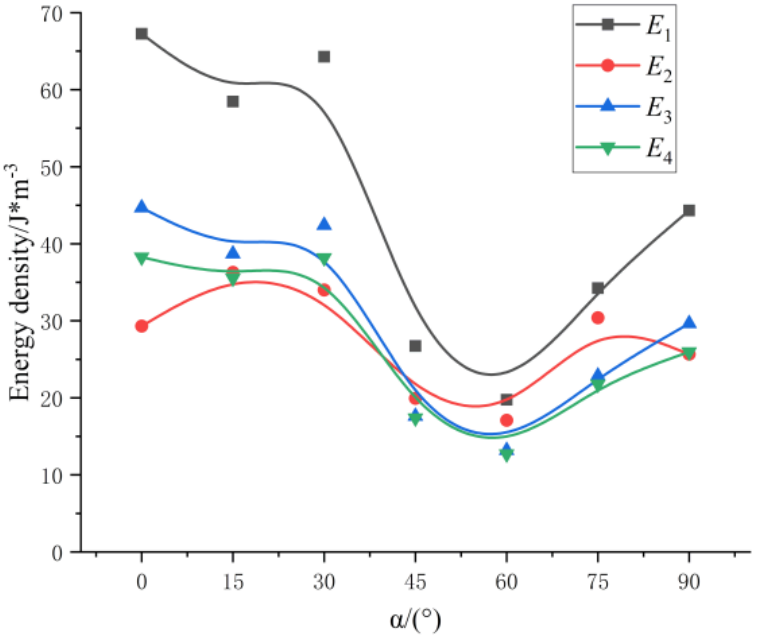

Figure 9. Characteristic energy fitting curves of coal rocks with different azimuths.

Table 4. Energy characteristic index of coal at different azimuth angles.

α(°)	Elastic Energy Index	Impact Energy Index	Effective Impact Energy Index	Residual Energy Index
0	5.95	36.27	15.80	14.80
15	11.21	16.30	10.11	9.11
30	9.06	20.36	10.77	9.77
45	27.14	3.11	2.32	1.32
60	23.13	2.10	1.81	0.81
75	20.19	3.84	3.41	2.41
90	7.03	12.66	7.33	6.33

3.3.2. Analysis of Acoustic Emission Characteristics during Coal Fracture Damage

In the numerical model, a fracture element represents an acoustic emission event, and the energy released by the fracture of the element is the acoustic emission energy. During the loading process, the accumulation of damage of the unit causes the overall damage of the macroscopic rock [47].

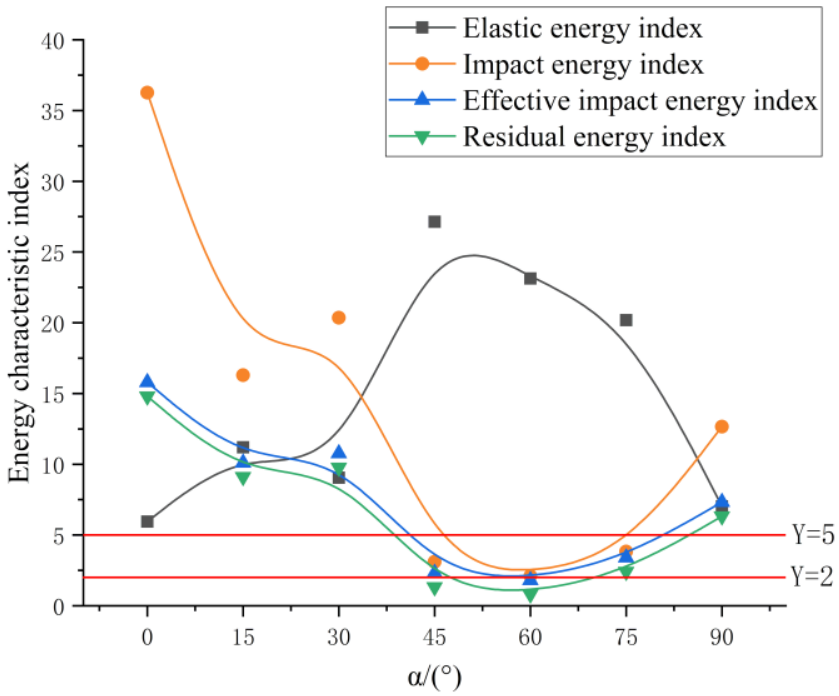

Figure 10. Characteristic energy index of coal at different azimuth angles.

The relationship between coal stress, acoustic emission energy, cumulative acoustic emission and acoustic emission count and loading steps under diverse azimuth is shown in Figures 11 and 12. Calcite veins have a substantial effect on the energy evolution in the process of coal damage. With the increase of azimuth, the energy evolution law changes, which can be roughly divided into two categories: the energy evolution law under low dip angle (0°, 15° and 30°) and the energy evolution law under high dip angle (45°, 60°, 75° and 90°). The specific analysis of energy evolution in the coal failure process under different azimuth angles is as follows:

- At low dip angles (0°, 15° and 30°), the compressive strength of coal is large, the stress required for fracture damage is large, the number of loading steps is large and more energy is released during coal and rock failure. When α = 0°, the maximum acoustic emission energy release is 149.9 J. From the AE counts, cumulative AE and acoustic emission energy curves, it is clear that the energy accumulation during coal rock destruction is slow when the calcite veins are at low angles. When the energy accumulation reaches its maximum, a large amount of accumulated energy is suddenly released and complete destruction of the coal rock occurs.
- At high dip angles (45°, 60°, 75° and 90°), the compressive strength of coal is small, the stress required for fracture damage is small, the number of loading steps is small and the energy released by coal failure is less. When α = 60°, the acoustic emission energy release is the smallest, which is 22.9 J. Compared with the 0° sample, the release energy decreases by 84.7%. The AE counts, cumulative AE and acoustic emission energy curves exhibited significant jumps. This is because under high dip angle, the stress distribution of coal and rock is uneven during loading, resulting in local failure of coal and rock, and finally the crack penetrates to form a macro single failure mode.

In conclusion, the fracture damage process of coal is significantly affected by calcite veins. Under low dip angle, the internal stress distribution of coal is relatively uniform, the weak cementation between coal matrix and calcite vein is not easy to be destroyed and the stress and energy required for coal destruction are large. Under high dip angle, the distribution of coal rock is uneven, and the weak cementation between coal matrix and calcite vein is easy to be damaged, resulting in coal fracture and damage.

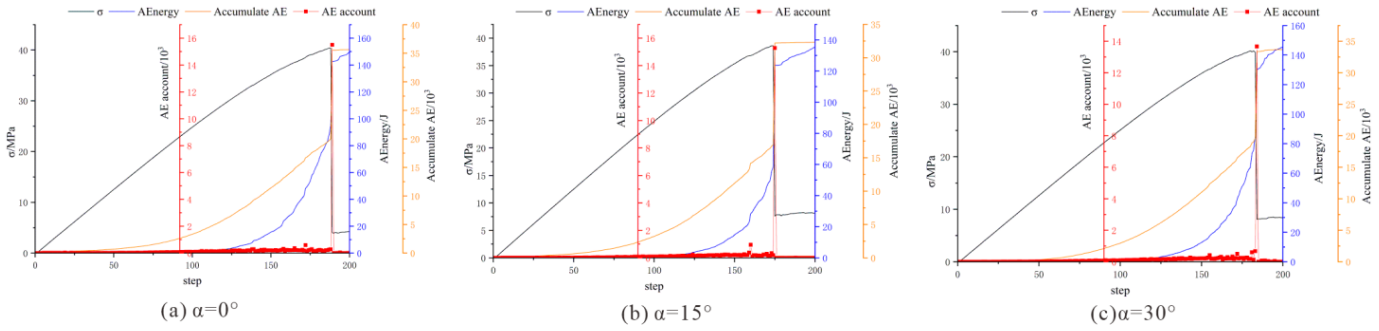

Figure 11. Relationship between loading stress, AE account, Accumulative AE and AEnergy and step number of coal under low dip angle.

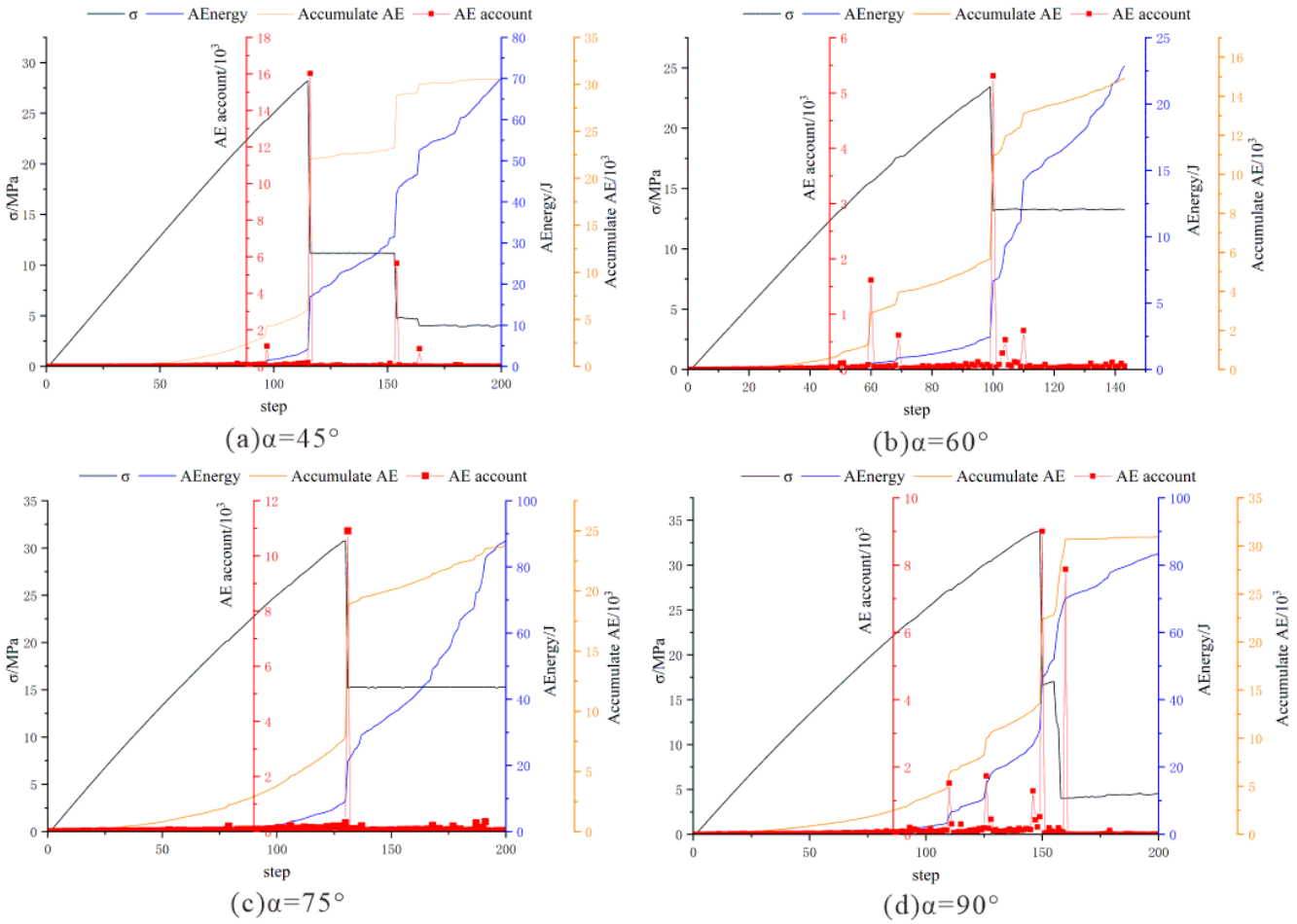

Figure 12. Relationship between loading stress, AE account, Accumulative AE and AEnergy and step number of coal under high dip angle.

4. Results and Discussion

In this study, the uniaxial compression test of coal rocks filled with calcite vein is carried out by using RFPA2D-DIP software, and the following beneficial results are obtained:

1. When the calcite vein has low dip angle (0°, 15° and 30°), the internal stress of coal rocks is mainly concentrated in the calcite vein under uniaxial compression, which is uniform and has high compressive strength. When α = 0°, the maximum compressive strength of coal rocks is 40.39 MPa. The final failure mode of coal rocks is complex, showing tensile failure and accompanied by more shear failure. In the process of uniaxial compression test, the input energy and accumulated elastic energy are larger,

the elastic energy index and impact energy index of coal rocks are larger and the energy released during failure is larger.

2. When the calcite vein has a high dip angle (45°, 60°, 75° and 90°), the internal stress of coal rocks is mainly concentrated in the calcite vein under uniaxial compression, but the distribution is uneven and the compressive strength is low. When $\alpha = 60°$, the compressive strength is the lowest, 23.45 MPa. The final failure mode of coal rocks is single, showing tensile failure accompanied by a small amount of shear failure. In the process of uniaxial compression test, the input energy and accumulated elastic energy are small, the elastic energy index and impact energy index of coal rocks are relatively small and the energy released during failure is low.

It can be seen from the above test results that a calcite vein has a significant impact on the mechanical properties, failure mode and energy evolution characteristics of coal. In the mining process, by artificially changing the angle between mining direction and calcite vein, the mechanical properties, failure mode and energy evolution characteristics of coal seam under the influence of mining can be changed, which can be used to control energy release disasters in the mining process and optimize mining technology. According to the test and analysis results, under high dip angles (45°, 60°, 75° and 90°), the coal compressive strength and energy release are low, and the mining is relatively safe.

5. Conclusions

In this study, uniaxial compression tests were conducted on coal rocks filled with calcite veins using RFPA2D-DIP software, and their mechanical properties and fracture damage energy evolution characteristics were analyzed, which can be summarized by the following rules:

1. The calcite vein-bearing coal rocks show strong anisotropic characteristics. The different azimuth angles of calcite veins change the internal stress distribution of coal, resulting in higher compressive strength of coal at low dip angle and lower compressive strength of coal at high dip angle.
2. The fracture mode of coal is significantly affected by calcite. At low dip angles (0°, 15° and 30°), the coal fracture modes are complex, which are inclined Z-type (0°), V-type (15°) and inverted V-type (30°) failure modes, respectively, and mainly shear failure. At high dip angles (45°, 60°, 75° and 90°), the fracture mode of coal and rock is single, which is type I failure mode, mainly tensile failure.
3. Calcite vein has a significant effect on energy evolution during coal fracture. At low dip angle, the input energy, accumulated elastic energy and impact energy index of coal are large. At high dip angle, the input energy, accumulated elastic energy and impact energy index of coal are low.
4. Calcite vein has a considerable impact on the fracture damage process of coal. Under low dip angle, the internal stress distribution of coal is relatively uniform, the weak cementation between coal matrix and calcite vein is not easy to be destroyed, and the stress and energy required for coal destruction are large. Under high dip angle, the internal distribution of coal is uneven, and the weak cementitious material between coal matrix and calcite vein is easy to be damaged, resulting in coal fracture and damage.

Author Contributions: Conceptualization, Z.W.; methodology, L.L.; software, Y.L.; writing—original draft preparation, W.W. All authors have read and agreed to the published version of the manuscript.

Funding: This study was supported by the Project of Special Fund for Science and Technology of The Guizhou Province Graduate Research Fund, the National Natural Science Foundation of China (Project Nos. 52104080, 51964007, 51774101), the High-Level Innovative Talents Training Project in Guizhou Province (Project No. 2016-4011), Project: Scientific Research Project of Guiyang Rail Transit Line 2 Phase I Project (Project No. D2(I)—FW—YJ—2019—001—WT), Teaching Reform Project of Guizhou University (Project No.JG201990), the Science and Technology Support Plan of Guizhou Province (Project No. [2021]401, [2020]4Y046, [2020]227), the Science and Technology Support Plan of

Guizhou Province (Science Support of Guizhou Province [2019] 2861) and the Science and Technology Project for Outing and Young Talents of Guizhou (Talents of Science Platform in Guizhou [2019] 5674).

Informed Consent Statement: Informed consent was obtained from all subjects involved in the study.

Conflicts of Interest: The authors declare no conflict of interest.

References

1. Su, X.; Lin, X.; Liu, S.; Zhao, M.; Song, Y. Geology of coalbed methane reservoirs in the Southeast Qinshui Basin of China. *Int. J. Coal Geol.* **2005**, *62*, 197–210. [CrossRef]
2. Galloway, W.E.; Hobday, D.K. Coal and Coalbed Methane. In *Terrigenous Clastic Depositional Systems*; Springer: Berlin/Heidelberg, Germany, 1996. [CrossRef]
3. Wang, G.X.; Massarotto, P.; Rudolph, V. An improved permeability model of coal for coalbed methane recovery and CO_2 geosequestration. *Int. J. Coal Geol.* **2009**, *77*, 127–136. [CrossRef]
4. Wei, Z.; Zhang, D. Coupled fluid flow and geomechanics in coalbed methane recovery study. *Mod. Phys. Lett. B* **2010**, *24*, 1291–1924. [CrossRef]
5. Feng, X.H.; Gong, B.; Tang, C.A.; Zhao, T. Study on the non-linear deformation and failure characteristics of EPS concrete based on CT-scanned structure modelling and cloud computing. *Eng. Fract. Mech.* **2022**, *261*, 108214. [CrossRef]
6. Senthamaraikkannan, G.; Budwill, K.; Gates, I.; Mitra, S.; Prasad, V. Kinetic Modeling of the Biogenic Production of Coalbed Methane. *Energy Fuels* **2016**, *30*, 871–883. [CrossRef]
7. Lu, B.; Shen, Y.; Tang, Z.; Zhang, D.; Chen, G. Vacuum pressure swing adsorption process for coalbed methane enrichment. *Chin. J. Chem. Eng.* **2021**, *32*, 264–280. [CrossRef]
8. Wang, H.; Liu, C. Process parameters design method of drainage gas recovery technology in gas-driven pump for coalbed methane production. *J. Pet. Sci. Eng.* **2021**, *207*, 109167.
9. Nie, B.; He, X.; Zhu, C. Study on mechanical property and electromagnetic emission during the fracture process of combined coal-rock. *Procedia Earth Planet. Sci.* **2009**, *1*, 281–287.
10. Huang, B.; Liu, J. The effect of loading rate on the behavior of samples composed of coal and rock. *Int. J. Rock Mech. Min. Sci.* **2013**, *61*, 23–30. [CrossRef]
11. Wang, Y.Y.; Gong, B.; Tang, C.A.; Zhao, T. Numerical study on size effect and anisotropy of columnar jointed basalts under uniaxial compression. *Bull. Eng. Geol. Environ.* **2022**, *81*, 41. [CrossRef]
12. Li, S.; Tang, D.; Xu, H.; Yang, Z. Advanced characterization of physical properties of coals with different coal structures by nuclear magnetic resonance and X-ray computed tomography. *Comput. Geosci.* **2012**, *48*, 220–227. [CrossRef]
13. Hou, L.; Liu, X.; Liang, L.; Xiong, J.; Zhang, P.; Xie, B.; Li, D. Investigation of coal and rock geo-mechanical properties evaluation based on the fracture complexity and wave velocity. *J. Nat. Gas Sci. Eng.* **2020**, *75*, 103133. [CrossRef]
14. Gong, B.; Liang, Z.Z.; Liu, X.X. Nonlinear deformation and failure characteristics of horseshoe-shaped tunnel under varying principal stress direction. *Arab. J. Geosci.* **2022**, *15*, 475. [CrossRef]
15. Zhu, Q.; Song, W.; Yang, Y.; Lu, X.; Liu, L.; Zhang, Y.; Sun, H.; Yao, J. An advection-diffusion-mechanical deformation integral model to predict coal matrix methane permeability combining digital rock physics with laboratory measurements. *Appl. Geochem.* **2021**, *126*, 104861. [CrossRef]
16. Kou, S.; Ye, D.; Ding, Y. A constitutive model for structured coal based on fracture and damage mechanics. *Eng. Fract. Mech.* **1990**, *35*, 614. [CrossRef]
17. Hao, X.; Du, W.; Jiang, Y.; Tannant, D.; Zhao, Y.; Guo, Y. Influence of bedding and cleats on the mechanical properties of a hard coal. *Arab. J. Geosci.* **2018**, *11*, 200. [CrossRef]
18. Xu, H.; Wang, G.; Fan, C.; Liu, X.; Wu, M. Grain-scale reconstruction and simulation of coal mechanical deformation and failure behaviors using combined SEM Digital Rock data and DEM simulator. *Powder Technol.* **2020**, *360*, 1305–1320. [CrossRef]
19. Liu, W.; Guo, Z.; Wang, C.; Niu, S. Physico-mechanical and microstructure properties of cemented coal Gangue-Fly ash backfill: Effects of curing temperature. *Constr. Build. Mater.* **2021**, *299*, 124011. [CrossRef]
20. Liu, X.S.; Tan, Y.L.; Ning, J.G.; Lu, Y.W.; Gu, Q.H. Mechanical properties and damage constitutive model of coal in coal-rock combined body. *Int. J. Rock Mech. Min. Sci.* **2018**, *110*, 140–150. [CrossRef]
21. Zhao, Z.; Wang, W.; Wang, L.; Dai, C. Compression-shear strength criterion of coal-rock combination model considering interface effect. *Tunn. Undergr. Space Technol.* **2015**, *47*, 193–199. [CrossRef]
22. Zhang, Y.; Feng, X.T.; Zhang, X.; Wang, Z.; Sharifzadeh, M.; Yang, C.; Kong, R.; Zhao, J. Strain energy evolution characteristics and mechanisms of hard rocks under true triaxial compression. *Eng. Geol.* **2019**, *260*, 105222. [CrossRef]
23. Wen, T.; Tang, H.; Ma, J.; Liu, Y. Energy Analysis of the Deformation and Failure Process of Sandstone and Damage Constitutive Model. *KSCE J. Civ. Eng.* **2019**, *23*, 513–524. [CrossRef]
24. Li, T.; Pei, X.; Wang, D.; Huang, R.; Tang, H. Nonlinear behavior and damage model for fractured rock under cyclic loading based on energy dissipation principle. *Eng. Fract. Mech.* **2019**, *206*, 330–341. [CrossRef]
25. Wang, Y.; Gao, S.H.; Li, C.H.; Han, J.Q. Energy dissipation and damage evolution for dynamic fracture of marble subjected to freeze-thaw and multiple level compressive fatigue loading. *Int. J. Fatigue* **2021**, *142*, 105927. [CrossRef]

26. Cornetti, P.; Pugno, N.; Carpinteri, A.; Taylor, D. Finite fracture mechanics: A coupled stress and energy failure criterion. *Eng. Fract. Mech.* **2006**, *73*, 2021–2033. [CrossRef]
27. Bratov, V.; Petrov, Y. Optimizing energy input for fracture by analysis of the energy required to initiate dynamic mode I crack growth. *Int. J. Solids Struct.* **2007**, *44*, 2371–2380. [CrossRef]
28. Ferro, G. On dissipated energy density in compression for concrete. *Eng. Fract. Mech.* **2006**, *73*, 1510–1530. [CrossRef]
29. Wang, Z.; Li, L. Study of Energy Release in Failure of Coal and Rock Near Fault on ANSYS. *Geotech. Geol. Eng.* **2019**, *37*, 2577–2589. [CrossRef]
30. Zhang, C.; Canbulat, I.; Tahmasebinia, F.; Hebblewhite, B. Assessment of energy release mechanisms contributing to coal burst. *Int. J. Min. Sci. Technol.* **2017**, *27*, 43–47. [CrossRef]
31. Lin, B.; Liu, T.; Zou, Q.; Zhu, C.; Yan, F.; Zhang, Z. Crack propagation patterns and energy evolution rules of coal within slotting disturbed zone under various lateral pressure coefficients. *Arab. J. Geosci.* **2015**, *8*, 6643–6654.
32. Gong, B.; Wang, Y.Y.; Zhao, T.; Tang, C.A.; Yang, X.Y.; Chen, T.T. AE energy evolution during CJB fracture affected by rock heterogeneity and column irregularity under lateral pressure. *Geomat. Nat. Hazards Risk* **2022**, *13*, 877–907. [CrossRef]
33. Dou, L.M.; Lu, C.P.; Mu, Z.L.; Gao, M.S. Prevention and forecasting of rock burst hazards in coal mines. *Min. Sci. Technol.* **2009**, *19*, 585–591. [CrossRef]
34. Yang, Z.; Liu, C.; Tang, S.; Dou, L.; Cao, J. Rock burst mechanism analysis in an advanced segment of gob-side entry under different dip angles of the seam and prevention technology. *Int. J. Min. Sci. Technol.* **2018**, *28*, 891–899. [CrossRef]
35. Lin, B.; Zhang, J.; Shen, C.; Zhang, Q.; Chen, S. Technology and application of pressure relief and permeability increase by jointly drilling and slotting coal. *Int. J. Min. Sci. Technol.* **2012**, *22*, 545–551. [CrossRef]
36. Xie, J.; Liang, Y.; Zou, Q.; Li, L.; Li, X. Elimination of coal and gas outburst risk of low-permeability coal seam using high-pressure water jet slotting technology: A case study in Shihuatian Coal Mine in Guizhou Province, China. *Energy Sci. Eng.* **2019**, *7*, 1394–1404.
37. Kwan, A.K.H.; Mora, C.F.; Chan, H.C. Particle shape analysis of coarse aggregate using digital image processing. *Cem. Concr. Res.* **1999**, *29*, 1403–1410. [CrossRef]
38. Yue, Z.Q.; Chen, S.; Tham, L.G. Finite element modeling of geomaterials using digital image processing. *Comput. Geotech.* **2003**, *30*, 375–397. [CrossRef]
39. Tang, C.; Tham, L.; Lee, P.; Yang, T.; Li, L. Coupled analysis of flow, stress and damage (FSD) in rock failure. *Int. J. Rock Mech. Min. Sci.* **2002**, *39*, 477–489. [CrossRef]
40. Lou, Y.; Wu, Z.; Sun, W.; Yin, S.; Wang, A.; Liu, H.; Zuo, Y. Study on failure models and fractal characteristics of shale under seepage-stress coupling. *Energy Sci. Eng.* **2020**, *8*, 1634–1649. [CrossRef]
41. Wu, Z.; Zuo, Y.; Wang, S.; Yi, T.; Chen, S.; Yu, Q.; Li, W.; Sunwen, J.; Xu, Y.; Wang, R.; et al. Numerical simulation and fractal analysis of mesoscopic scale failure in shale using digital images. *J. Pet. Sci. Eng.* **2016**, *145*, 592–599. [CrossRef]
42. Hou, L.L.; Liu, X.J.; Liang, L.X.; Zhang, P.; Xie, B.; Li, D. Numerical simulation of effect of cleats on energy evolution of coal and rock in loading process. *J. China Coal Soc.* **2020**, *45*, 1061–1069. (In Chinese) [CrossRef]
43. Jaeger, J.C. *Rock Mechanics and Engineering*; Cambridge University Press: London, UK, 1979.
44. Bai, T.; Pollard, D.D. Fracture Spacing in Layered Rocks: A New Explanation Based on the Stress Transition. *J. Struct. Geol.* **2000**, *22*, 43–57. [CrossRef]
45. Tang, C.A.; Zhang, Y.B.; Liang, Z.Z.; Xu, T.; Tham, L.G.; Lindqvist, P.A.; Kou, S.Q.; Liu, H.Y. Fracture spacing in layered materials and pattern transition from parallel to polygonal fractures. *Phys. Rev. E* **2006**, *73 Pt 2*, 056120. [CrossRef]
46. Zhang, Z.; Gao, F.; Cui, Y.; Lin, B. Association of Energy Characteristics and Meso-structure of Rock. *Sci. Technol. Rev.* **2013**, *31*, 20–26. (In Chinese)
47. Liang, Z.Z.; Tang, C.A.; Li, H.X.; Zhang, Y.B. Numerical simulation of the 3D failure process in heterogeneous rocks. *Int. J. Rock Mech. Min. Sci.* **2004**, *41*, 419. [CrossRef]